

Normalised Multi-Jet Cross Sections at High Q^2 using Regularised Unfolding and Extraction of $\alpha_s(M_Z)$ in Deep-Inelastic Scattering at HERA

H1 Collaboration

Abstract

New results on normalised inclusive jet, dijet and trijet differential cross sections in neutral current deep-inelastic ep scattering (DIS) based on a regularised unfolding procedure are presented. Detector effects like acceptance and migrations as well as statistical correlations between the multijets and the inclusive DIS events are taken into account in this procedure. The DIS phase space of this measurement with the H1 detector is given by the virtuality of the exchanged boson (γ^*, Z^0) $150 < Q^2 < 15000 \text{ GeV}^2$ and the inelasticity of the interaction $0.2 < y < 0.7$. The jets are reconstructed in the Breit frame of reference using the inclusive k_T jet algorithm. In all cases the jet pseudorapidities in the laboratory frame are required to be in the range $-1.0 < \eta_{lab} < 2.5$. For inclusive jets the transverse momenta in the Breit frame are $7 < P_T < 50 \text{ GeV}$. The dijet and trijet phase space are defined by requiring $5 < P_{T,i} < 50 \text{ GeV}$, and the invariant mass of the two leading jets $M_{1,2} > 16 \text{ GeV}$. Compared to a previously published result on normalised multijet cross sections, the new features are an extended range in jet pseudorapidity, an improved hadronic energy scale uncertainty of 1% and the adoption of a regularised unfolding procedure. The unfolded normalised jet cross sections are compared to QCD calculations at NLO and values for the strong coupling $\alpha_s(M_Z)$ are extracted.

1 Introduction

Jet production in neutral current (NC) deep-inelastic scattering (DIS) at HERA provides an important testing ground for Quantum Chromodynamics (QCD). While inclusive DIS gives only indirect information on the strong coupling via scaling violations of the proton structure functions, the production of jets allows a direct measurement of α_s and can further constrain the gluon density in parton distribution functions (PDFs). Typically one distinguishes between inclusive jet measurements, where each single jet is counted, and exclusive jet measurements like dijet and trijet measurements, where each event is counted that fulfills topological and kinematic criteria on jet quantities. Both approaches allow to extract the strong coupling by comparing to theoretical predictions.

The data-theory comparison and the determination of the strong coupling is typically performed on hadron level. Thus, data have to be corrected for detector effects and theory for hadronisation effects. While the latter are determined using MC event generators, ideally using various hadronisation models, the correction of detector effects is called *unfolding* and corrects for kinematic migrations due to finite resolution and limited acceptance of the detector.

2 Phase Space

This document extends the preliminary analysis as presented in [1]. Only a brief summary of the kinematic region of the measurement is given here.

The selected NC DIS events, computing the kinematics from the measurements of the scattered electron and the hadronic final state, fulfill the following requirements:

$$150 < Q^2 < 15000 \text{ GeV}^2 \quad \text{and} \quad 0.2 < y < 0.7,$$

with Q^2 being the virtuality of the exchanged vector boson (γ^*/Z^0) and $y = Q^2/(s x_{\text{Bj}})$ the inelasticity of the interaction (s being the centre-of-mass energy and x_{Bj} being the Bjorken scaling variable).

The jet finding is performed in the Breit frame of reference, where the proton collides head on with the exchanged boson, which is at rest. Particle candidates in the hadronic final state are clustered into jets using the inclusive k_{T} algorithm [2] with a distance parameter $R_0 = 1$, as implemented in FastJet [3].

The phase space for the inclusive jets is given by

$$-1.0 < \eta_{\text{lab}} < 2.5,$$

where η_{lab} is the jet pseudorapidity in the laboratory frame, and the transverse momentum of a jet in the Breit frame P_{T} is in the range between:

$$7 < P_{\text{T}} < 50 \text{ GeV}.$$

Events with at least two (three) jets with transverse momentum larger than 5 GeV are considered as dijet (trijet) events. In order to avoid regions of phase-space where fixed order perturbation theory is not reliable [4], dijet events are accepted only if the invariant mass M_{12} of the two leading jets exceeds 16 GeV. The same requirement, $M_{12} > 16$ GeV, is applied to the trijet events so that the trijet sample is a subset of the dijet sample. For events that fulfill the dijet (trijet) criteria the average transverse momentum $\langle P_T \rangle = \frac{1}{N} \sum_i^N P_T^{\text{jet},i}$ ($N = 2$ or 3) is defined as an observable.

The inclusive jets (dijets, trijets) are measured in bins of Q^2 and P_T of the jets ($Q^2, \langle P_T \rangle$) and are normalised to the inclusive DIS measurement in the respective bins of Q^2 . The advantages of these normalised jet cross sections compared to absolute jet cross sections are reduced systematic experimental uncertainties as well as the Parton Distribution Function (PDF) uncertainty.

3 Detector Correction and Regularised Unfolding

Due to kinematic migrations, because of finite resolution and limited acceptance of the detector, the data have to be corrected for these effects. For this purpose a multidimensional regularised unfolding procedure, including all correlations, is applied. This procedure makes use of a migration matrix A that connects the *particle level* that is represented by a vector x with the *detector level*, represented by a vector y . While the folding, given by the detector response, i.e. the migration matrix A , acting on the generator level distribution can be represented by the linear equation

$$y = A \cdot x,$$

the unfolding cannot generally be accomplished simply by matrix inversion. Large fluctuations of the result may arise, resulting from small singular values/eigenvalues that appear as well as numerical limitations of the eigenvalue spectrum when inverting the response matrix.

The regularised unfolding method, as implemented in TUNFOLD [5], solves this problem by introducing a regularisation condition with a tiny regularisation parameter τ . The particle level vector is then determined by an analytical minimisation of a χ^2 function as function of x . This function reads

$$\chi^2(x) = (y - A \cdot x)^T V_{yy}^{-1} (y - A \cdot x) + \tau^2 (x - x_0)^T (L^T L) (x - x_0), \quad (1)$$

where A is the migration matrix, x is the to be determined particle level vector, y is the measured detector level vector, and V_{yy} is its covariance matrix. The regularisation parameter τ and L determine the regularisation condition, and x_0 is the bias distribution. In our case L is set to the unity matrix.

The essential part of the unfolding is to construct a matrix in such a way that all kinematical migrations are respected. For all relevant observables, the rule of thumb is followed of having approximately 1.5 to 2 times more bins on detector level than on particle level. In addition, the bins on detector level are chosen to be commensurate to the resolution of the respective observable. Furthermore, the phase space is extended in all kinematic variables, to take migrations into and out of the phase space into account. These additional bins are called *side-bins*.

Two different Monte Carlo event generators, DJANGO [6] and RAPGAP / [7] are employed, after reweighting of some distributions to obtain a good description of the measurements, to build two migration matrices. The average of both is used for the data unfolding. Both models are leading order (LO) event generators matched with parton showers and interfaced with the Lund string fragmentation model [8]. The DJANGO event generator uses the color dipole model (CDM) with QCD matrix element corrections as implemented in ARIADNE [9]. The RAPGAP event generator is based on QCD matrix elements matched with parton showers in the leading log approximation. All generated events are processed using a `Geant3` [10] based simulation of the H1 apparatus and in the following are treated by the same analysis chain as data.

3.1 Inclusive Jet Migration Matrix

The inclusive jet measurement is performed double differentially in Q^2 and P_T . The relevant observables for the migrations are identified to be Q^2 and P_T . Also migrations in η_{lab} could be relevant. The inclusive jet measurement is special as it is a measurement of jet-multiplicities. Jets are defined on detector level and on particle level, separately. In order to define matching jets on both levels, a closest pair algorithm with a distance measure

$$R = \sqrt{\Delta\phi^2 + \Delta\eta^2}$$

is used, where $\Delta\phi$ is the angular separation of two jets in the xy-plane (in the H1 coordinate system) and $\Delta\eta$ is the separation in η_{lab} between the two analysis levels. This distance measure does not introduce any kinematic assumptions and thus is free of biases in kinematic variables. In order not to match spatial opposite jets, a maximum distance of $R < 0.9$ between two jets is demanded. The algorithm looks iteratively for the closest pair of all combinatorial pairs of jets on the two levels. Using this jet matching criterion, three kinds of jets can be distinguished:

- **Matched jets**

Matched jets are all jets which have a matching jet, and all variables are defined on detector and particle level. The matched jets describe the kinematical migrations and are used to construct up the migration matrix.

- **Particle-level-only jets**

Particle-level-only jets are jets, which are on particle level but could not be matched to any jet on detector level. This may be due to acceptance effects, e.g. if essential constituents of this jet go into non-instrumented parts of the detector, or due to kinematic migrations, especially of jets with low transverse momentum. The particle-level-only jets are treated like acceptance effects in the migration matrix.

- **Detector-level-only jets**

Detector-level-only jets are jets in Monte Carlo events which are found on detector level but no jet matches on particle level. The event is well-defined on detector level, and all NC DIS kinematic variables are determined. This gives the opportunity, to determine the amount of detector-level-only jets from the measured inclusive NC DIS observables.

The migration matrix describing the detector response for the inclusive jet measurement is set up three-dimensionally in the kinematic variables y , Q^2 and $P_{T,\text{jet}}$. In each y bin a separate $P_{T,\text{jet}}$ migration matrix is determined, and for each bin in this matrix a migration matrix in Q^2 is determined. The kinematic region and the number of bins of the migration matrix are given in table 2. Each matched jet is filled into one bin of the migration matrix and connects the reconstructed level with the particle level. In addition, the migration matrix is extended in each particle level bin by one bin for the normalisation, where contributions from acceptance effects, trigger efficiencies and the particle-level-only jets are filled into.

Aside from the migration matrix for the inclusive jets, a separate migration matrix for the inclusive NC DIS measurement is set up. This migration matrix is two-dimensionally in the variables y and Q^2 , and the same binning as for the inclusive jets is used.

The two migration matrices are set into the diagonal elements of a 2×2 matrix. One of the diagonal elements connects the inclusive jet measurement on particle level with the inclusive NC DIS measurement on detector level. This matrix is used to determine the amount of detector-level-only jets within the reconstructed inclusive jet data from the measured inclusive NC DIS events. The second off-diagonal element of the 2×2 matrix is empty, because the unfolded inclusive jet measurement shall only be determined by measured jet quantities.

3.2 Dijet Migration Matrix

The dijet measurement is performed double differentially in Q^2 and $\langle P_T \rangle$. Events are counted which fulfill topological criteria, kinematic constraints on individual jets and on combined jet quantities. In addition, migrations into and out of these criteria are taken into account here.

An event is classified as a dijet event, if the selection criteria as given in table 1 are fulfilled. There are also events with two jets, where not all selection criteria are fulfilled. These events, which do not fulfill all selection criteria but only some on one level can migrate into the selection on the other level. Therefore, these events play an important role in the unfolding.

The dijet migration matrix has a three-dimensional structure in the observables y , Q^2 and $\langle P_T \rangle$. Each bin of the y migration matrix contains a Q^2 migration matrix and each bin in Q^2 contains a $\langle P_T \rangle$ migration matrix. The $\langle P_T \rangle$ matrix-scheme is extended on generator and particle level to include the migrations into and out of the defined dijet selection. These additional bins contain events, which have at least two jets in the kinematic region of $5 < P_{T,\text{jet}} < 50$ GeV and which are separated into events with an invariant mass above or below 16 GeV and for $\langle P_T \rangle$ above or below 7 GeV. One additional bin counts events in an extended phase space, which extend the possible phase space for dijet events by extending the cut on jets in η_{lab} to the range $-1.5 < \eta_{\text{lab}} < 2.75$.

3.3 Trijet Migration Matrix

The trijet measurement is performed double differentially in Q^2 and $\langle P_T \rangle$. The unfolding scheme is very similar to the dijet unfolding scheme, where all $\langle P_T \rangle$ are substituted by trijet $\langle P_T \rangle$. Compared to the dijet migration matrix the number of bins in the trijet migration matrix is reduced to obtain sufficient statistic in all relevant bins, and the phase space is reduced,

since no significant number of events with a $\langle P_T \rangle > 30$ GeV can be observed because of the requirement of $P_{T,\text{jet}} < 50$ GeV.

3.4 The Migration Matrix

The full migration matrix has the overall structure of a 4×4 matrix, where the diagonal elements are the migration matrices of the four individual measurements. The three sub-matrices that connect the detector level jet data to the particle level inclusive NC DIS data, are used to estimate the inclusive jets, but also dijet and trijet events, which fulfill the dijet/trijet criteria only on detector level but not on particle level. Such migrations take mostly place in events with low- P_T jets, where migrations out of the respected phase space of the unfolding occur. All other nine sub-matrices are empty. This procedure ensures that only the reconstructed data of a certain jet measurement determines its particle level distribution. In addition to the overall 4×4 structure, each particle level bin has a normalisation bin which contains the efficiency corrections and the generator-level-only jets or events. The normalisation bins of the inclusive NC DIS measurement receive further negative entries to correct for the additional content from the detector-level-only entries of the jet measurements. Overall, the migration matrix has 2205 bins on reconstructed level and 671 bins on particle level.

3.5 Testing the Unfolding Using Monte Carlo Events

Several checks on the unfolding procedure are performed. The technical correctness of the migration matrix is checked by performing the *folding* process analytically by confirming the equality

$$y \equiv A \cdot x.$$

It is expected that the unfolding process does not introduce a systematic shift. This assumption is confirmed by unfolding a Monte Carlo pseudo-data set, which is generated with the same Monte Carlo program as the unfolding matrix. The pseudo data are generated with comparable statistics as the real data and are statistically independent of the unfolding matrix. A pull value p_i for each bin i on generator level is defined by the unfolded value x_i , the true value on particle level x_i^{true} , and the statistical error after the unfolding Δx_i , by

$$p_i = \frac{x_i - x_i^{\text{true}}}{\Delta x_i}. \quad (2)$$

The pull values of all phase-space bins of the inclusive jet (24 bins), the dijet (24 bins) and the trijet measurements (17 bins) are shown in fig. 1 for DJANGO and RAPGAP and are compared to a bin-by-bin corrected prediction that also employs statistical independent samples. For all N phase space bins a mean pull value is defined as $\langle p \rangle = \frac{1}{N} \sum_i p_i$. The mean values of the individual measurements are well compatible with zero and thus the unfolding procedure does not introduce any systematic shift.

An unfolding where the pseudo data are generated by one model and the migration matrix by the other model is also performed. The two employed models are based on different physics assumptions (matrix-element plus parton shower or color-dipole model) and they also predict slightly different spectra on generator level. This test gives valuable information on the universality of the unfolding scheme. The pull distributions, where once the pseudo data are generated by DJANGO and the unfolding matrix is generated by RAPGAP and vice-versa, are shown in fig. 2. The pull distribution for the bin-by-bin corrected cross sections are shown for comparison. The mean values are shifted but are significantly closer to zero for the unfolded result than for the bin-by-bin corrected one. The unfolding is able to reduce the model dependence compared to the bin-by-bin correction method. Nevertheless, there is still some residual model dependence and therefore an uncertainty on this model dependence has to be determined for the final result. The model uncertainty is determined the same way as other systematic uncertainties (see sec. 4), by employing alternative migration matrices, which are determined once by DJANGO and once by RAPGAP only.

3.6 Unfolding procedure

The unfolding is performed using TUNFOLD v17.beta4, which minimises eq. 1 and analytically determines the particle level distribution x . The variables y and V_{yy} are given by the data, where y is the background subtracted data, and V_{yy} is the covariance matrix of the measurement including the correlated uncertainties on the background subtraction. The average of the migration matrices of the two models A_{DJANGO} and A_{RAPGAP} is used as migration matrix

$$A = \frac{A_{\text{DJANGO}} + A_{\text{RAPGAP}}}{2}.$$

The regularisation condition, represented by the matrix L in eq. 1 is chosen to be a unity matrix, and the estimated underlying distribution x_0 is determined by the projection of the migration matrix.

Before the actual unfolding step a high- y contribution is subtracted the same way as background is treated. This contribution is estimated by the employed models and accounts for events that are generated at $y_{\text{gen}} > 0.7$, but are reconstructed in the final phase-space $y_{\text{rec}} < 0.7$. This contribution cannot be reasonably determined by data, since the scattered electron energy must fulfill $E_e > 11$ GeV leading to an insignificant amount of data in that region.

The regularisation parameter τ is determined using the L-Curve method [11] to

$$\tau = 8.07 \cdot 10^{-6}.$$

The variation of the regularisation parameter within a reasonable range does not change the unfolded cross sections. A too large regularisation parameter pushes the unfolded result to zero, since the regularisation condition using the unity matrix is enforcing this behaviour.

The χ^2 is determined to be

$$\chi_A^2 = 2030$$

and

$$\chi_L^2 = 197.0,$$

where χ_A^2 refers to the first summand in eq. 1 containing the $(y - Ax)$ part and χ_L^2 being the second summand representing the regularisation condition.

The covariance matrix V_{xx} of the unfolded result on particle level is determined by an error propagation of the input covariance matrix V_{yy} . The unfolded data and their covariance matrix are corrected for radiative effects applying a bin-by-bin correction as in [1].

3.7 Unfolded result

The applied unfolding procedure determines the inclusive NC DIS cross sections single differentially and the inclusive jet, the dijet and trijet cross sections double differentially. Single differential and absolute cross sections can be determined by adding corresponding bins. The unfolded cross sections are compatible with the bin-by-bin corrected cross sections in [1] within the statistical errors. The statistical error of the unfolded cross sections is larger compared to the bin-by-bin corrected cross sections, because all migrations were included in the error calculation. However, this comparison is misleading, since the statistical error of the unfolded cross sections is a correlated error, while the bin-by-bin correction neglects these correlations. The unfolding procedure generates also negative correlations between bins where migrations take place. Correlated bins can therefore show large errors on plots and suggest a low precision, but are very precise when these bins are used together in a fit which incorporates the full covariance matrix. The correlation coefficient K_{ij} between two bins i and j is calculated from the covariance matrix V by

$$K_{ij} = \frac{V_{ij}}{\sqrt{V_{ii} \cdot V_{jj}}} \quad (3)$$

and gives the strength of the correlation between two bins.

The correlation matrix K_{ij} of all four measurements is shown in fig. 3. The correlations result from three different sources:

- The unfolding procedure corrects the data for kinematical migrations and therefore generates negative correlations between bins where migrations take place. These are typically large in bins which are small compared to the resolution. Negative correlations are most obvious in neighboring P_T or $\langle P_T \rangle$ bins of the inclusive jet measurement or of the dijet and trijet measurement, respectively. The resolution in Q^2 compared to the size of the bins is better than for jet quantities, and therefore the negative correlations resulting from Q^2 -migrations are typically smaller between neighboring Q^2 bins than for P_T bins.
- The same data are used for all four measurements and therefore the measurements are positively correlated to each other. Correlation are measured by determining the full covariance matrix of the data and are then propagated through the unfolding procedure.

- The P_T bins within one Q^2 bin of the inclusive jet measurement are positively correlated since multiple jets are counted within a single event. Therefore, positive correlations on detector level are measured between P_T bins, but different bins in Q^2 are always uncorrelated. However, those correlations cannot be seen in the correlation matrix after the unfolding, since the negative correlations resulting from the unfolding are larger.

Pull values p between the unfolded and the bin-by-bin corrected cross sections of all phase space bins are calculated and are shown in fig. 4. The unfolded cross sections are shifted by $\langle p \rangle = -0.8 \pm 0.1$ against the bin-by-bin corrected result. Since the Monte Carlo test has shown that the unfolding compared to the bin-by-bin correction method incorporates a smaller model bias, we can conclude that the unfolded cross sections give more reliable results and are less dependent on model predictions.

4 Experimental uncertainties

The same sources of experimental uncertainties are considered as in [1]. For each source of uncertainty two migration matrices are determined to account for up and down variations of this source. The two models are added to determine the average matrix of the systematic source i , and can be written as $A_{\text{sys},i} = A + \Delta A_{\text{sys},i}$, where $\Delta A_{i,\text{sys}}$ is the difference to the nominal unfolding matrix. The uncertainty $\Delta x_{\text{sys},i}$ on each source of uncertainty is determined by a linearised error propagation of the shifted migration matrices through the unfolding procedure by the replacements in eq. 1:

$$\begin{aligned} A &\rightarrow A + \Delta A_{\text{sys},i} \\ x &\rightarrow x + \Delta x_{\text{sys},i} \end{aligned}$$

5 Hadronisation corrections

Corrections factors for hadronisation effects are calculated using Monte Carlo event generators. To determine the corrections the same procedure as in [1] is followed, but the error on the hadronisation correction is calculated differently. SHERPA [12], a Monte Carlo event generator based on multi-leg LO matrix elements is used and is interfaced once to the the string fragmentation model [8] and once the cluster fragmentation model [13]. The difference of the prediction by the two hadronisation models is used as an uncertainty on the hadronisation correction.

6 Determination of normalised cross sections

The unfolding procedure provides jet cross sections and inclusive NC DIS cross sections, and therefore the normalised jet cross sections are not measured directly on detector level but are determined from the unfolded cross sections on particle level. Each bin of a jet measurement is normalised to the corresponding bin of that Q^2 of the inclusive DIS measurement. The

covariance matrix of all the normalised jet measurements can be determined by a full error propagation. It comprises the errors and the covariances of the normalised inclusive jet, the normalised dijet and the normalised trijet measurements. Also the covariances between bins of different measurements are determined, and therefore all three normalised measurements can be used together in a combined fit (see sec. 8.3). This procedure is equivalent to a direct measure of normalised jet cross sections, but has the advantage of the direct determination of all correlations.

7 NLO QCD prediction of jet cross sections

Perturbative QCD (pQCD) predictions for the jet cross sections at the parton level are calculated using the NLOJET++ program [14, 15] which is interfaced to FASTNLO [16, 17]. The calculation is performed in next-to-leading order (NLO) in the strong coupling constant and using the \overline{MS} scheme with five massless quark flavors. The strong coupling constant is evolved in two loop precision. The partons are grouped to jets using the same jet definition as in the data analysis. When comparing data and theory predictions the strong coupling constant is chosen to be $\alpha_s(M_Z) = 0.118$ at the Z^0 mass and the CT10 PDF set [18] is used. The renormalisation scale is set to $\mu_r = \sqrt{(P_T^2 + Q^2)}/2$, where $\langle P_T \rangle$ is used instead of P_T in the case of the dijet and trijet measurements. The factorisation scale is set to Q .

The calculation of the inclusive DIS cross sections is performed using the QCDNUM program [19]. The calculation does not include QED radiation effects or Z^0 exchange contributions, but the running of the electromagnetic coupling with Q^2 is taken into account. The calculation is performed in the massless 'zero mass variable flavor number scheme' (ZM-VFNS) in analogy to the massless calculation of jet cross sections. No contribution of the Z^0 exchange is included since the contribution cancels for the normalised jet cross sections.

8 Results

The double differential cross sections of the normalised inclusive jets, the normalised dijet and normalised trijet measurement are presented and the strong coupling constant is extracted. A comparison between the unfolded and bin-by-bin corrected cross sections is presented further.

8.1 Cross section measurements compared to NLO predictions

The normalised inclusive jet cross sections as a function Q^2 and P_T are shown in fig. 5 and are compared to NLO predictions on hadron level. The six pads show the four P_T bins for each of the six Q^2 bins, as well as the ratio $\sigma_{\text{NLO}}/\sigma_{\text{data}}$. The inner error bars depict the statistical errors and the outer error bars show all systematic error sources added quadratically to the statistical error. The correlation of the statistical error of one bin to another bin cannot be seen in these plots. The error band on the NLO cross section shows the uncertainty arising from variations

of the renormalisation and the factorisation scale by a factor of 2 up and down. The normalised dijet and the normalised trijet cross sections as a function of Q^2 and $\langle P_T \rangle$ are shown in fig. 6 and fig. 7, respectively.

The statistical errors are effectively reduced when the correlations between the data points are taken into account. The correlation matrix which is used to determine the normalised jet cross sections is shown in fig. 3. The correlations between bins of the normalised cross sections are quite similar to the correlations of the absolute cross sections, since the correlations of the inclusive NC DIS measurements after the unfolding are small and similar migrations in Q^2 occur in all four measurements.

All three normalised jet measurements can be used together in a fit since the correlation matrix is known and this analysis presents one single analysis. The three normalised jet measurements are shown together with the NLO predictions in fig. 8.

8.2 Unfolded vs. bin-by-bin corrected normalised cross sections

Normalised jet cross sections are also determined by applying the bin-by-bin correction technique for the correction of detector effects. These cross sections are compared to the unfolded cross sections by calculating the ratio with respect to the unfolded cross section. The ratios are shown for the three normalised jet measurements in figs. 9, 10 and 11 where also the NLO calculations are depicted.

Pull values are calculated between the unfolded and the bin-by-bin corrected cross sections. A staggered plot of these pull values of all phase-space bins is shown in fig. 4. The normalised cross sections obtained with the two different correction methods are compatible within the statistical uncertainty. However, the unfolded cross sections tend to be lower than the bin-by-bin corrected cross sections.

8.3 Extraction of the Strong Coupling

The QCD predictions for jet production depend directly on α_s and on the parton density functions of the proton. For the determination of the strong coupling the CT10 PDF set is used.

The strong coupling is determined by performing a χ^2 -minimisation procedure with $\alpha_s(M_Z)$ as a free parameter. The minimisation algorithm MIGRAD is used as implemented in the MINUIT [20] program, where the errors on the fit parameters are equivalent to the hessian errors. Here, the implementation TMINUIT is used as provided by the ROOT analysis framework [21].

While the calculations of jet cross sections in NLO can take considerable time, the FASTNLO program provides an efficient method to calculate these cross sections. It stores the perturbative coefficients from NLOJET++ in an efficient way and multiplies them with the PDFs and $\alpha_s(\mu_T)$. Thus, the cross section calculation can be repeated very fast, and the strong coupling can be determined in an iterative fit. The inclusive DIS cross sections are calculated using QCDNUM

as described in sec. 8.1.

The χ^2 definition follows [22] and was similarly used in global data analyses [23] and also in previous H1 publications [24, 25]. Nuisance parameters for each source of systematic uncertainty are introduced and are treated as free parameters in the fit. All nuisance parameters are well distributed around zero for the minimal χ^2 . The usage of the covariance matrix enables to use all three normalised jet measurements together. The uncertainties on the electron energy and on the hadronic energy scale are split up and 50% are treated as correlated uncertainties using nuisance parameters, and 50% are added quadratically to the diagonal elements of the covariance matrix. The experimental uncertainty on $\alpha_s(M_Z)$ is given by an increase in χ^2 of one unit with respect to the minimal value.

Uncertainties on the derived strong coupling, which do not result from the data uncertainties are also determined. These include uncertainties on the theory prediction, on the hadronisation correction and on the PDFs. They are treated with the so called *offset* method, where the fit is repeated with theory predictions shifted by an offset of the size of the uncertainty. The difference between the nominal fit and the shifted fit is defined to be the error arising from this uncertainty on the values determined by the fit. These errors are given separately to the resulting $\alpha_s(M_Z)$ value and experimental uncertainty since they are basically independent of the precision of the H1 data and experience considerable improvement in the future.

The uncertainty on the theory cross section is determined conventionally by varying the renormalisation and factorisation scales. For each of the two scales a scan is performed, where in every bin the largest and lowest cross section prediction is determined (denoted *up* and *down* error) in the range of a multiplicative scale factor between 0.5 and 2.0. The scales are varied for the inclusive NC DIS cross sections as well as for the jet cross section predictions by the same factor. Since QCDNUM cannot change the factorisation scale independently from the renormalisation scale, in the case the factorisation scale variation it is assumed that the impact of the variation of the renormalisation scale on the NC DIS cross section can be neglected. The up-errors on the variation of the renormalisation scale and on the factorisation scale are added in quadrature to determine the theory up-error. The down-error is calculated analogously.

The uncertainty on the theory cross section arising from the limited knowledge of the PDF is determined for one single PDF set following the PDF4LHC recommendation [26]. For each pair of eigenvectors of the CT10 PDF set, the up and down error is determined in each bin. All up or down errors in each bin are added in quadrature to obtain the total up and down error, respectively, on the cross section arising from the PDF uncertainty. This method probably overestimates the PDF uncertainty since it ignores correlations between bins. Surprisingly, the PDF error is not reduced for the normalised jet cross sections, but is even slightly increased compared to the jet cross sections. This is essentially a consequence of the PDF sum rules. If e.g. the gluon density in a certain PDF eigenvector set is increased, the valence and sea quark densities are decreased. It follows that jet cross sections increase while the inclusive NC DIS cross sections decrease, because to the different sensitivity on certain parton densities and thus the uncertainty on the normalised cross sections resulting from this particular eigenvector is increased.

The uncertainty on the cross sections arising from limited knowledge of the hadronisation correction is explained in more detail in section 5.

The strong coupling constant $\alpha_s(M_Z)$ is determined for each of the three normalised jet cross section measurements individually as well as for all three simultaneously. The values obtained and the uncertainties due to the sources are discussed and given in table 4. The individual fits to measurements show a good χ^2/ndf of around unity. The extracted $\alpha_s(M_Z)$ value from the normalised inclusive jets is 0.1197 ± 0.0008 and from the normalised dijets it is 0.1142 ± 0.0010 . These values, while indicating some tension, are compatible within the theoretical uncertainty of about 0.005 and are also compatible with previous H1 publications [24, 25] and with the world average [27].

The simultaneous fit to the three normalised jet cross sections shows a large $\chi^2/\text{ndf} = 105/64$. Since the results on $\alpha_s(M_Z)$ from the normalised inclusive jets and the normalised dijets showed some tension, a large χ^2/ndf is expected. Although both measurements incorporate the same dataset, the observables P_T and $\langle P_T \rangle$ are different. The analysis and various checks suggest that the inclusive jet and dijet data are consistent, and thus the difference in $\alpha_s(M_Z)$ is assumed to arise from the theoretical cross section predictions. The k -factor which is defined as the ratio of the cross section calculated in NLO and LO $k = \sigma_{\text{NLO+LO}}/\sigma_{\text{LO}}$, is an indicator for missing higher orders in the QCD calculation. In order to ensure that observables have a small dependence on (missing) higher orders, we repeat the simultaneous fit to the three normalised jet cross section measurements using only bins with k -factors smaller 1.3. The resulting fit takes contributions from 42 bins out of a total of 65 into account and shows a reasonable χ^2/ndf of 53/41. The resulting $\alpha_s(M_Z)$ is determined to be

$$\alpha_s(M_Z) = 0.1163 \pm 0.0008 \text{ (exp.)} \pm 0.0011 \text{ (had.)} \pm 0.0014 \text{ (pdf)} \begin{matrix} +0.0044 \\ -0.0035 \end{matrix} \text{ (theo.)}.$$

The result is consistent with previous results in H1 publications [24]. The theoretical uncertainties from missing higher orders, the PDF uncertainty and the hadronisation corrections are significantly larger than experimental uncertainty.

9 Conclusion

Measurements of normalised inclusive jet, normalised dijet and normalised trjet cross sections in the Breit frame in NC DIS in the range $150 < Q^2 < 15000 \text{ GeV}^2$ and $0.2 < y < 0.7$ using the H1 data taken during the HERA-2 running are presented. The obtained jet cross sections are corrected using a regularised unfolding procedure for detector effects and taking correlations into account. Next-to-leading order calculations provide a good description of the measurements, and a value of $\alpha_s(M_Z)$ is extracted from a simultaneous fit to all three normalised measurements.

Acknowledgements

We are grateful to the HERA machine group whose outstanding efforts have made this experiment possible. We thank the engineers and technicians for their work in constructing and maintaining the H1 detector, our funding agencies for financial support, the DESY technical staff for continual assistance and the DESY directorate for support and for the hospitality which they extend to the non DESY members of the collaboration.

References

- [1] H1 Collaboration, “Measurement of Multijet Production in Deep-Inelastic ep Scattering at high Q^2 at HERA ,” *preliminary result: H1prelim-11-032* (2011) .
- [2] S. D. Ellis and D. E. Soper, “Successive combination jet algorithm for hadron collisions,” *Phys. Rev. D* **48** (1993) 3160.
- [3] M. Cacciari and G. P. Salam, “Dispelling the N^3 myth for the k_T jet-finder,” *Phys. Lett. B* **641** (2006) 57.
- [4] S. Frixione and G. Ridolfi, “Jet photoproduction at HERA,” *Nucl. Phys.* **B5 07** (1997) 315.
- [5] S. Schmitt, “TUnfold: an algorithm for correcting migration effects in high energy physics,” arXiv:1205.6201 [physics.data-an].
- [6] K. Charchula, G. Schuler, and H. Spiesberger, “Combined QED and QCD radiative effects in deep inelastic lepton-proton scattering: The Monte Carlo generator DJANGO6,” *Comput. Phys. Commun.* **81** (1994) 381.
- [7] H. Jung, “Hard diffractive scattering in high energy ep collisions and the Monte Carlo generator RAPGAP,” *Comput. Phys. Commun.* **86** (1995) 147.
- [8] B. Andersson, G. Gustafson, G. Ingelman, *et al.*, “Parton fragmentation and string dynamics,” *Phys. Rep.* **97** (1983) 31.
- [9] L. Lönnblad, “Ariadne version 4 – A program for simulation of QCD cascades implementing the colour dipole model,” *Comput. Phys. Commun.* **71** (1992) 15.
- [10] R. Brun, F. Bruyant, M. Maire, *et al.*, “GEANT: Simulation Program for Particle Physics Experiments. User Guide and Reference Manual,” *CERN-DD/EE 84-1* (1987) .
- [11] P. C. Hansen, “The l-curve and its use in the numerical treatment of inverse problems,” in *Computational Inverse Problems in Electrocardiology*, ed. P. Johnston, *Advances in Computational Bioengineering*, pp. 119–142. WIT Press, 2000.
- [12] T. Gleisberg, S. Hoeche, F. Krauss, *et al.*, “Event generation with SHERPA 1.1,” *JHEP* **0902** (2009) 007, arXiv:0811.4622 [hep-ph].

- [13] J.-C. Winter, F. Krauss, and G. Soff, “A Modified cluster hadronization model,” *Eur.Phys.J.* **C36** (2004) 381–395, arXiv:hep-ph/0311085 [hep-ph].
- [14] Z. Nagy and Z. Trocsanyi, “Next-to-leading order calculation of four-jet observables in electron-positron annihilation,” *Phys. Rev. D* **59** (1999) 14020.
- [15] Z. Nagy and Z. Trocsanyi, “Multijet Cross Sections in Deep Inelastic Scattering at Next-to-Leading Order,” *Phys. Rev. Lett.* **87** (2001) 82001.
- [16] T. Kluge, K. Rabbertz, and M. Wobisch, “FastNLO: Fast pQCD calculations for PDF fits,” 2006. arXiv:hep-ph/0609285 [hep-ph].
- [17] M. Wobisch, D. Britzger, T. Kluge, and others title =.
- [18] H.-L. Lai, M. Guzzi, J. Huston, *et al.*, “New parton distributions for collider physics,” *Phys.Rev.* **D82** (2010) 074024, arXiv:1007.2241 [hep-ph].
- [19] M. Botje, “A QCD analysis of HERA and fixed target structure function data,” *Eur. Phys. J. C* **14** (2000) 285.
- [20] F. James and M. Roos, “Minuit: A System for Function Minimization and Analysis of the Parameter Errors and Correlations,” *Comput.Phys.Commun.* **10** (1975) 343–367.
- [21] R. Brun and F. Rademakers, “Root an object oriented data analysis framework,” *Nuclear Instruments and Methods in Physics Research Section A: Accelerators, Spectrometers, Detectors and Associated Equipment* **389** no. 1-2, (1997) 81–86.
- [22] C. Pascaud and F. Zomer, “QCD analysis from the proton structure function F2 measurement: Issues on fitting, statistical and systematic errors,” LAL-95-05.
- [23] V. Barone, C. Pascaud, and F. Zomer, “A New global analysis of deep inelastic scattering data,” *Eur.Phys.J.* **C12** (2000) 243–262, arXiv:hep-ph/9907512 [hep-ph].
- [24] H1 Collaboration, F. Aaron *et al.*, “Jet Production in ep Collisions at High Q^{*2} and Determination of $\alpha(s)$,” *Eur.Phys.J.* **C 65** (2010) 363–383, arXiv:0904.3870 [hep-ex].
- [25] H1 Collaboration, F. Aaron *et al.*, “Jet Production in ep Collisions at Low Q^{*2} and Determination of $\alpha(s)$,” *Eur.Phys.J.* **C 67** (2010) 1–24, arXiv:0911.5678 [hep-ex].
- [26] S. Alekhin, S. Alioli, R. D. Ball, *et al.*, “The PDF4LHC Working Group Interim Report,” arXiv:1101.0536 [hep-ph].
- [27] S. Bethke, “The 2009 world average of α_s ,” *Eur. Phys. J. C* **64** (2009) 689–703.

NC DIS Selection	$150 < Q^2 < 15000 \text{ GeV}^2 \quad 0.2 < y < 0.7$		
Inclusive jet	$7 < P_T < 50 \text{ GeV}$		$-1.0 < \eta_{\text{lab}} < 2.5$
Dijet	$5 < P_T^{\text{jet1}}, P_T^{\text{jet2}} < 50 \text{ GeV}$	$M_{12} > 16 \text{ GeV}$	
Trijet	$5 < P_T^{\text{jet1}}, P_T^{\text{jet2}}, P_T^{\text{jet3}} < 50 \text{ GeV}$		

Table 1: Selection criteria for the NC DIS and jet samples.

Variable	#bins detector level	#bins particle level	Lower bound	Upper bound
y	3	2 (+1)	0.08	gen: 1.0, rec: 0.7
Q^2	15	8	120 GeV	40000 GeV
$P_{T,\text{jet}}$	10	6	3 GeV	100 GeV
$\langle P_T \rangle_{\text{Dijet}}$	10	6	3 GeV	50 GeV
$\langle P_T \rangle_{\text{Trijet}}$	8	5	3 GeV	30 GeV

Table 2: Kinematic range and number of bins of migration matrix for unfolding.

Bin number	Q^2 range (in GeV^2)	Bin label	P_T or $\langle P_T \rangle$ range (in GeV)
1	$150 \leq Q^2 < 200$	α	$7 \leq P_T < 11$
2	$200 \leq Q^2 < 270$	β	$11 \leq P_T < 18$
3	$270 \leq Q^2 < 400$	γ	$18 \leq P_T < 30$
4	$400 \leq Q^2 < 700$	δ	$30 \leq P_T < 50$
5	$700 \leq Q^2 < 5000$		
6	$5000 \leq Q^2 < 15000$		

Table 3: The bins in Q^2 , P_T or $\langle P_T \rangle$ for inclusive jets, dijets and trijets as shown in the following figures.

Measurement	$\alpha_s(M_Z)$	Uncertainty				χ^2/ndf
		experimental	had.	theory	PDF	
normalised inclusive jet	0.1197	0.0008	0.00118	+0.0054 -0.0053	0.0014	28.663/23 = 1.246
normalised dijet	0.1142	0.0010	0.0009	+0.0050 -0.0046	0.0017	27.037/23 = 1.176
normalised trijet	0.1185	0.0018	0.0016	+0.0050 -0.0035	0.0013	12.013/16 = 0.751
normalised multijet	0.1177	0.0008	0.0011	+0.0052 -0.0049	0.0014	104.61/64 = 1.634
normalised multijet ($k < 1.3$)	0.1163	0.0011	0.0008	+0.0044 -0.0035	0.0014	53.257/41 = 1.299

Table 4: The values of $\alpha_s(M_Z)$ fitting the individual measurements and fitting simultaneously all three normalised multijet measurements. The determination of $\alpha_s(M_Z)$ fitting simultaneously all the three measurements, however requiring a k -factor < 1.3 which results in taking only 42 measurement bins out of 65.

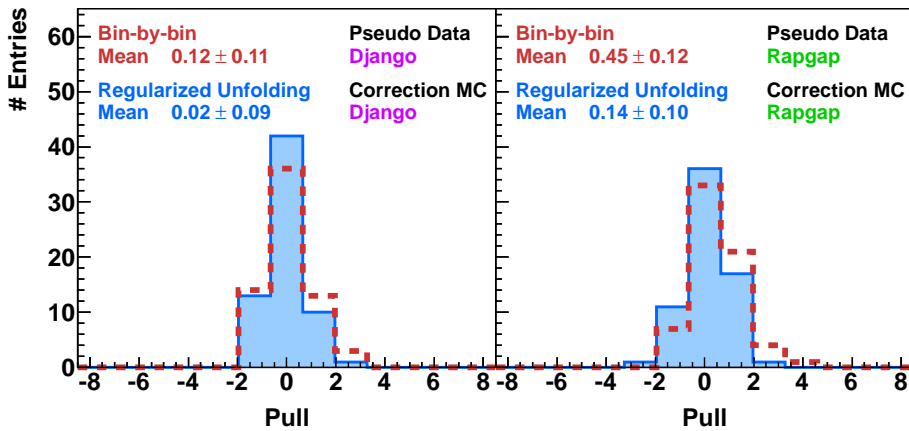


Figure 1: Pull values of unfolded pseudo-data and true pseudo-data for all phase space bins for a Monte Carlo unfolding using statistically independent events. For comparison also the pull values using the bin-by-bin corrected pseudo-data and the true pseudo-data are shown.

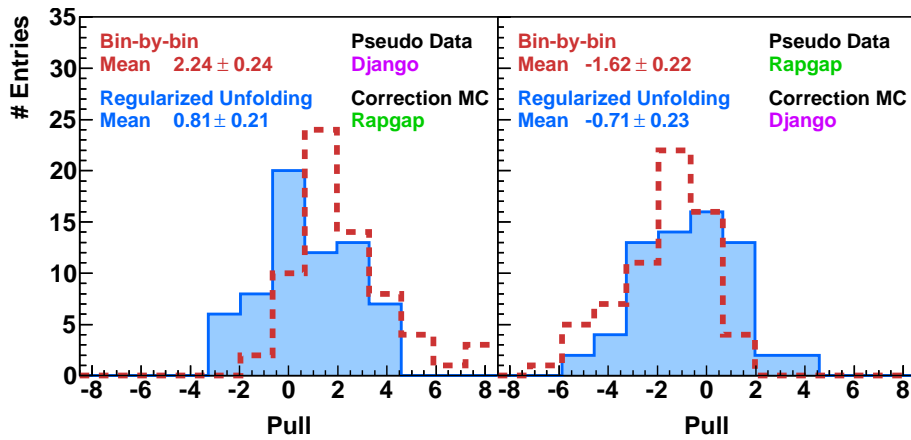


Figure 2: Pull values of unfolded pseudo-data and true pseudo-data for all phase space bins where the unfolding matrix was generated with a different MC models than the pseudo-data. For comparison the pull values using the bin-by-bin corrected pseudo-data are shown.

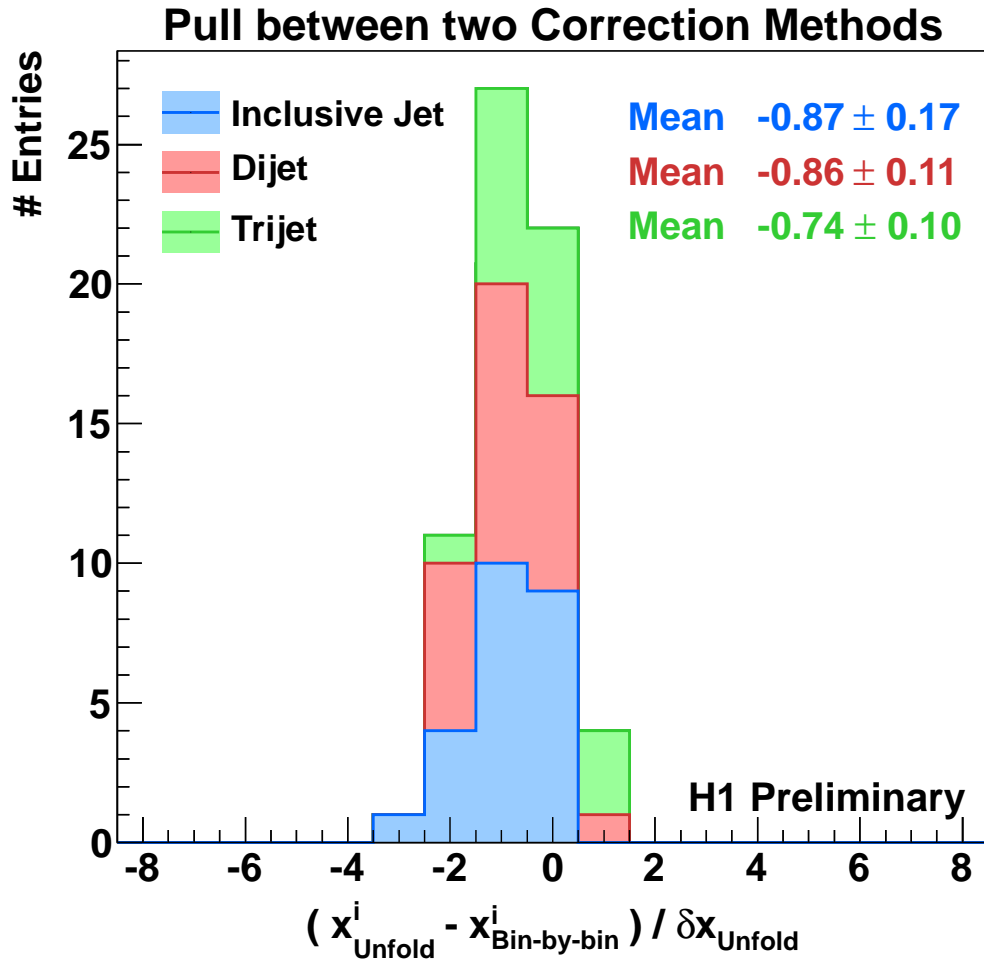


Figure 4: Pull values of the unfolded inclusive jet, dijet and trijet data vs the bin-by-bin corrected data.

Normalised Inclusive Jet Cross Section

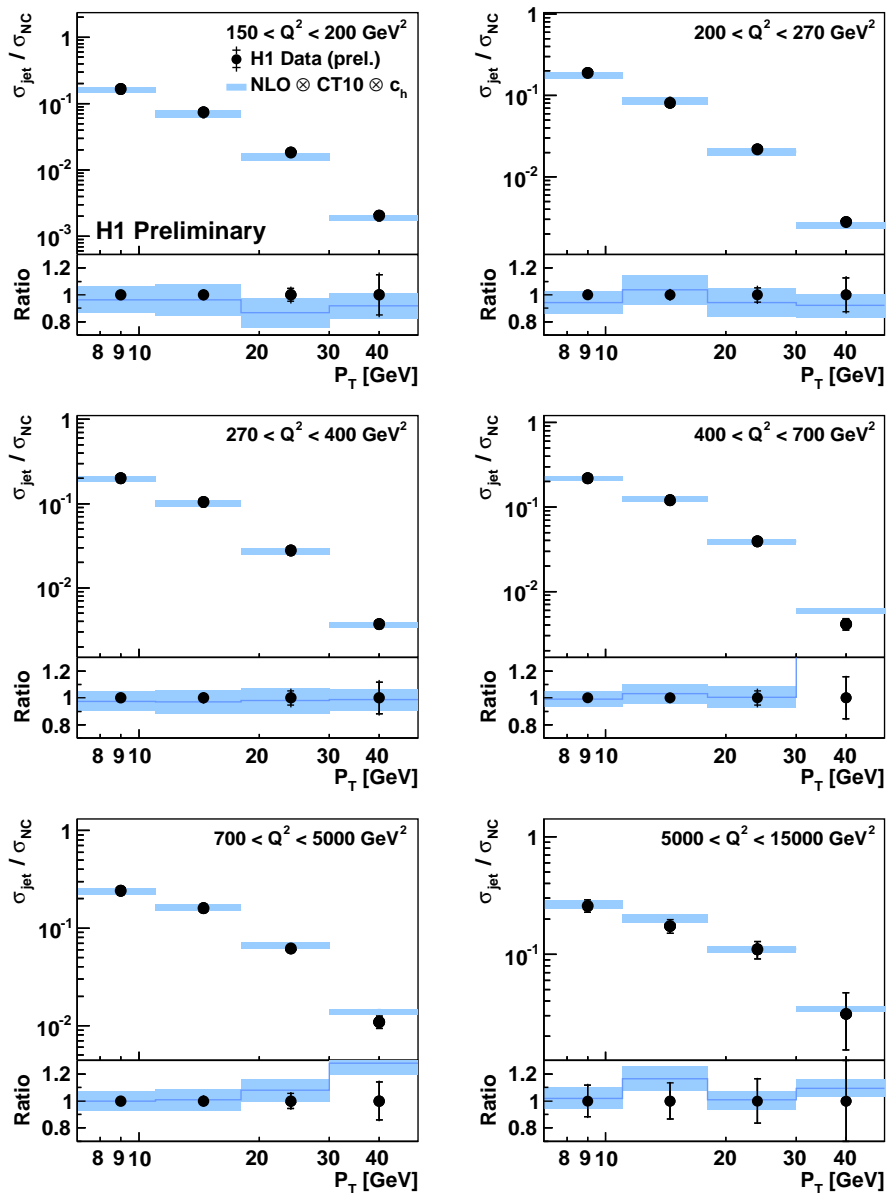


Figure 5: The normalised inclusive jet cross sections as functions of Q^2 and the transverse momentum in the Breit frame P_T . The inner error bars represent the statistical uncertainty. The correlations of the statistical uncertainties cannot be seen in this plot but in the correlation matrix in fig. 3. The NLO QCD predictions are shown with the symmetrised theory uncertainties determined by scale variations. The ratio of NLO QCD with respect to data is shown in the lower part of each plot.

Normalised Dijet Cross Section

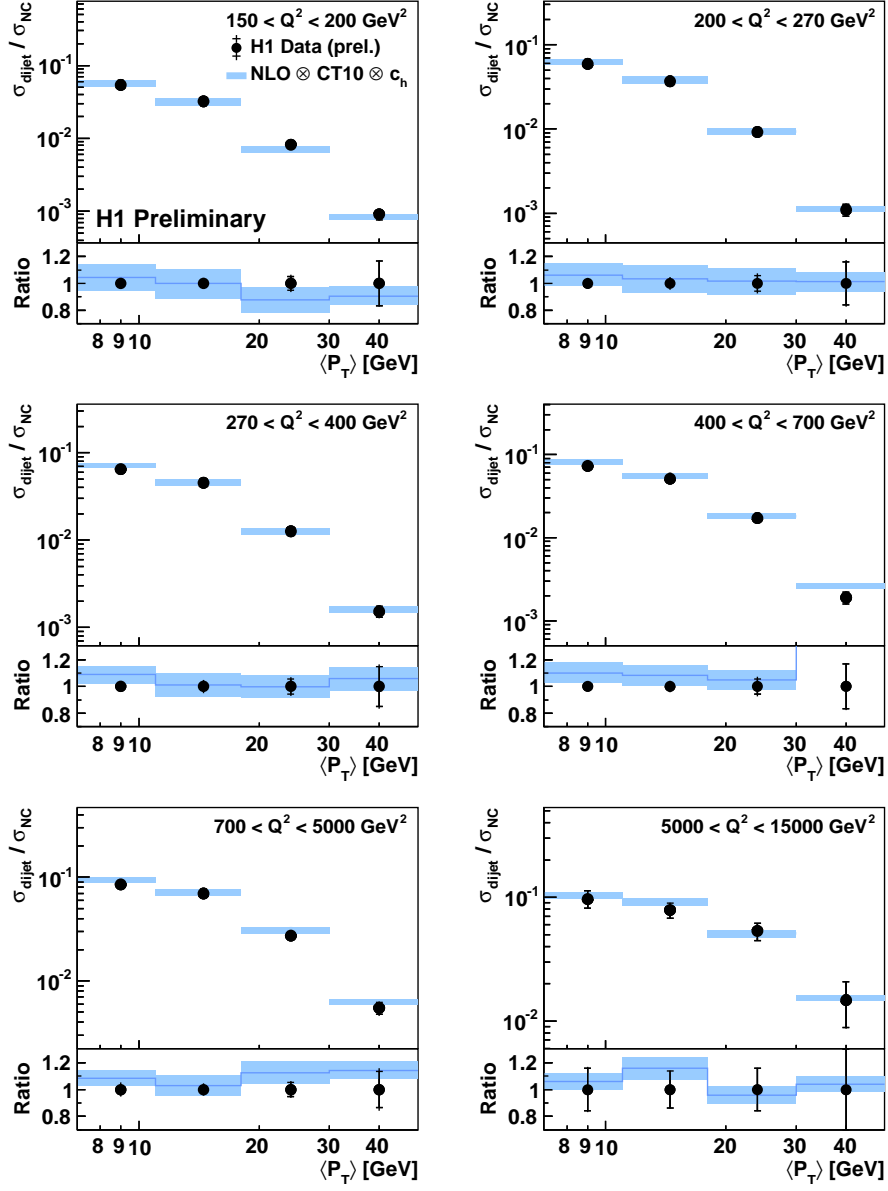


Figure 6: The normalised dijet cross sections in NC DIS as a function of the average transverse momentum of the two leading jets $\langle P_T \rangle$ in the Breit frame in the phase space as defined in table 1 in bins of Q^2 .

Normalised Trijet Cross Section

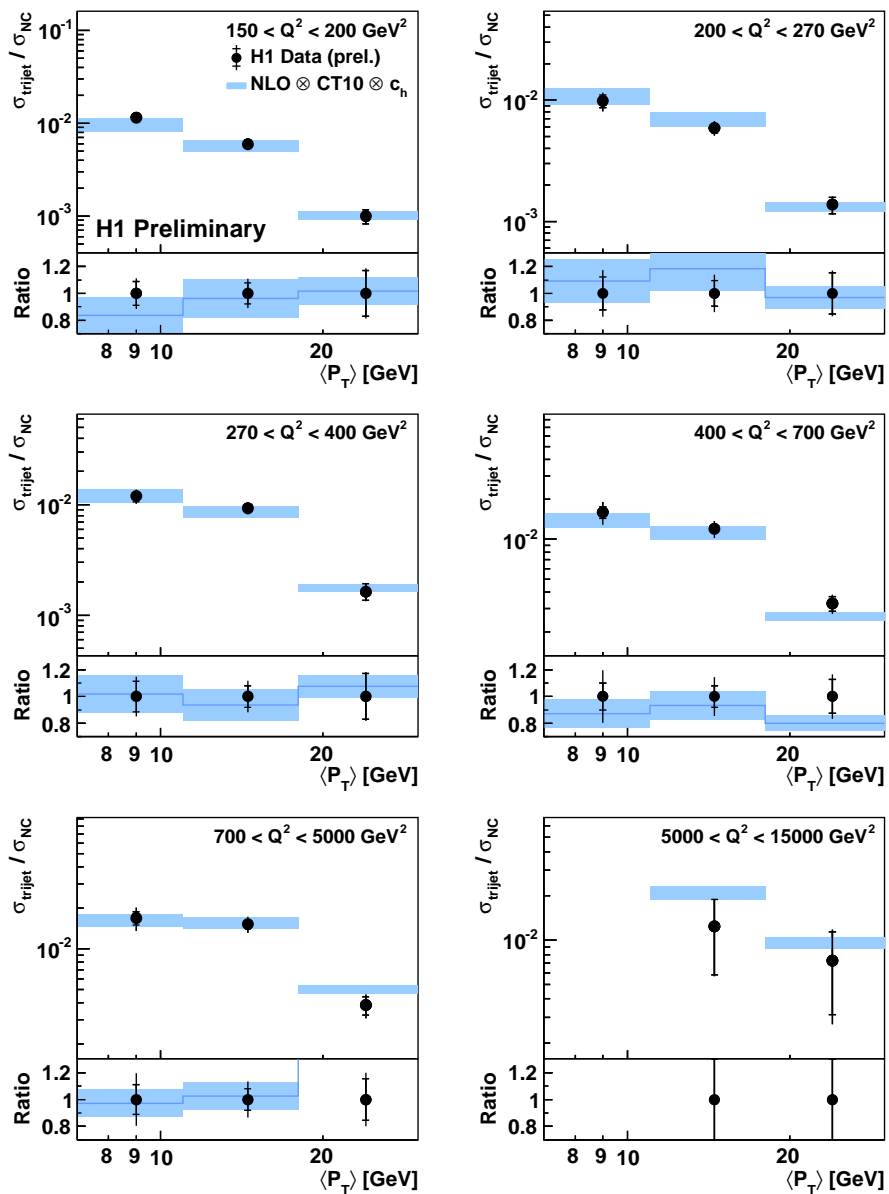


Figure 7: The normalised trijet cross sections in NC DIS as a function of the average transverse momentum of the three leading jets $\langle P_T \rangle$ in the Breit frame in the phase space as defined in table 1 in bins of Q^2 .

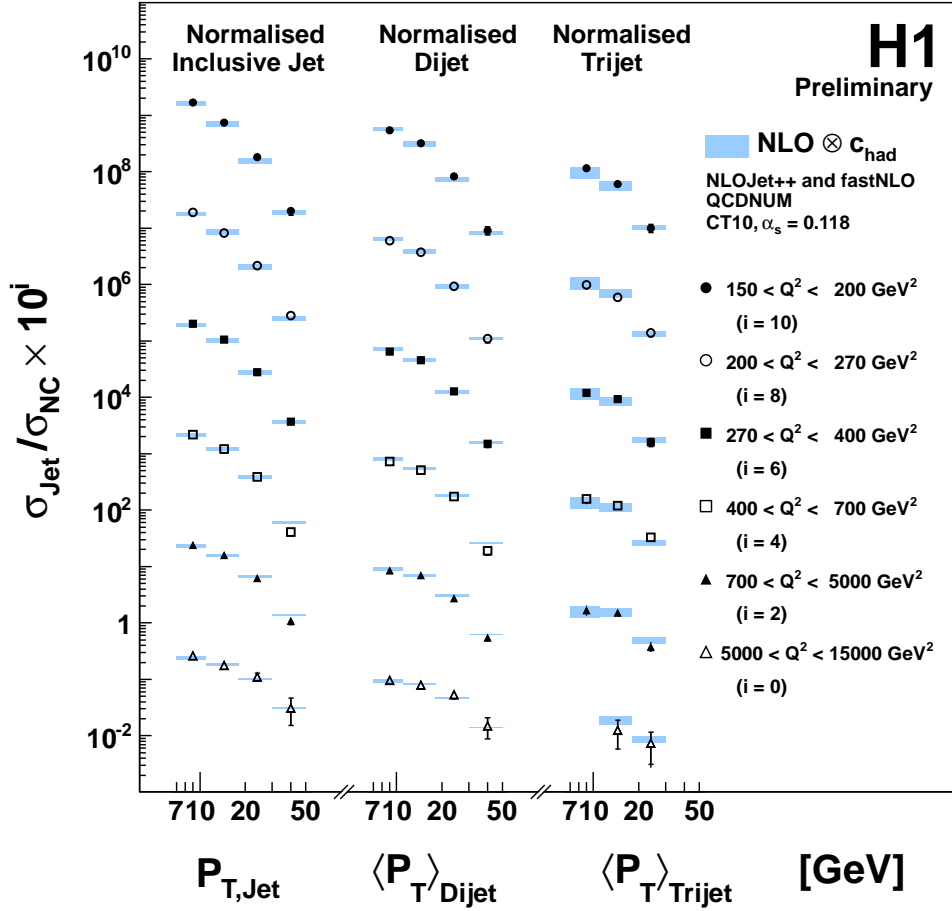


Figure 8: Normalised inclusive jet cross sections as functions of Q^2 and P_T and normalised dijet and normalised trijet cross section as function of Q^2 and $\langle P_T \rangle$ with comparison to NLO QCD predictions by NLOJET++ and QCDNUM using the CT10 PDF set and $\alpha_s(M_Z) = 0.118$.

Normalised Inclusive Jet Cross Section

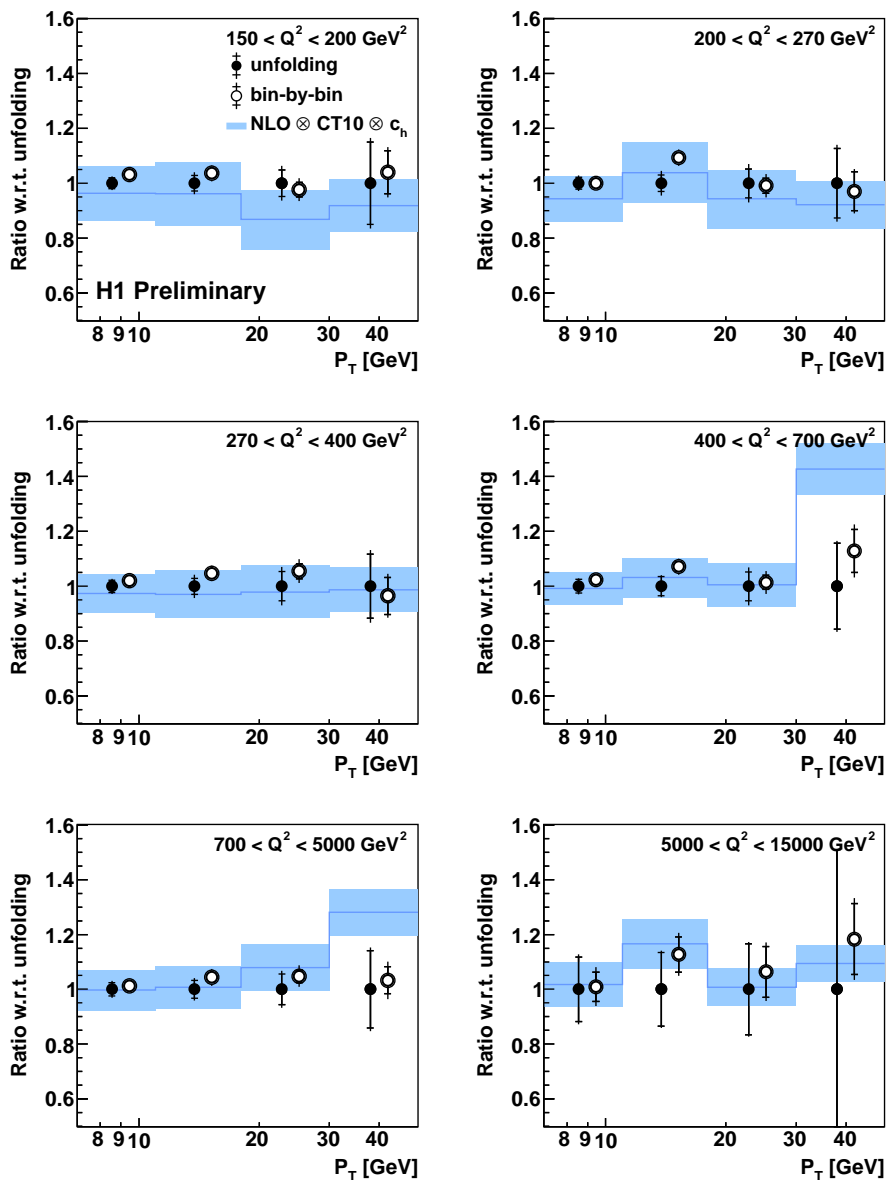


Figure 9: Ratio of the bin-by-bin corrected cross section of the normalised inclusive jets vs. the unfolded cross sections. For comparison also the ratio of the QCD prediction vs. the unfolded cross section is shown. The errors are shown in analogy to 5.

Normalised Dijet Cross Section

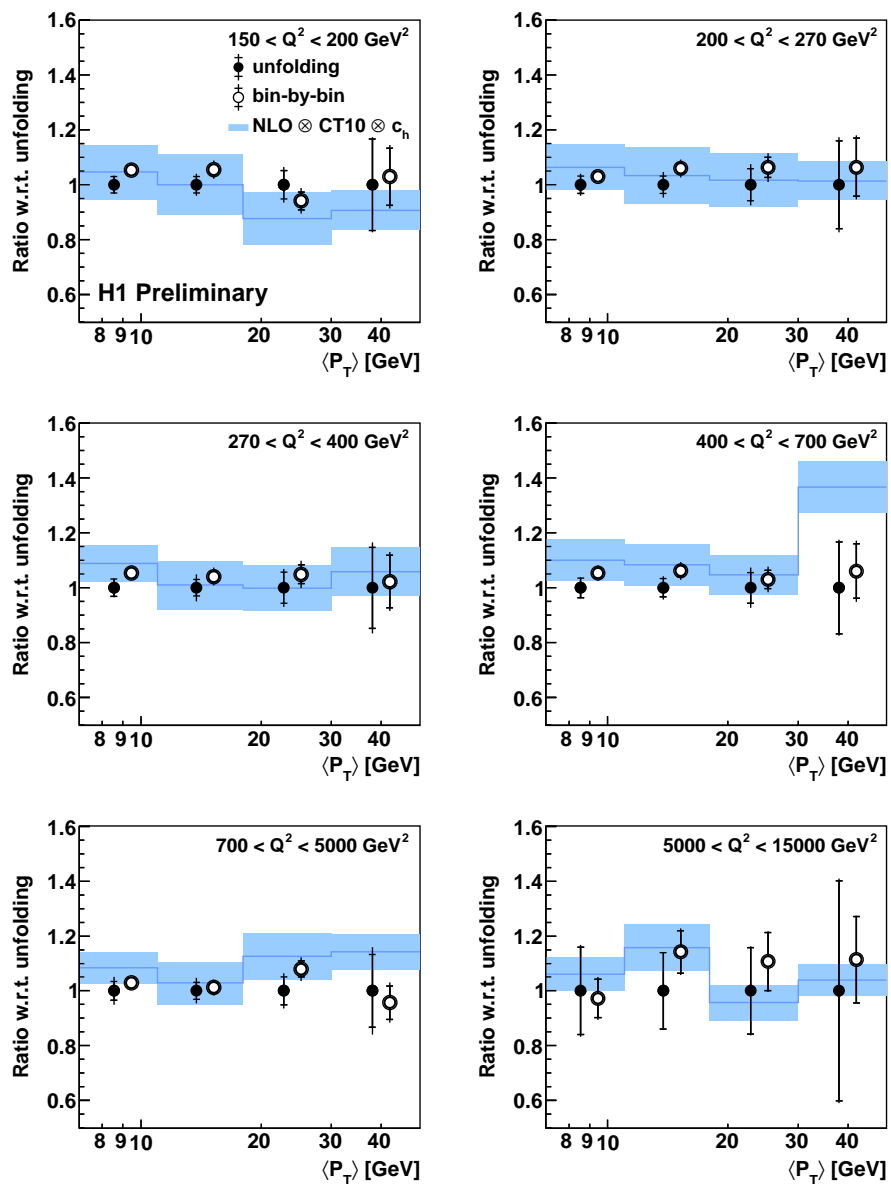


Figure 10: Ratio of the bin-by-bin corrected cross section of the normalised dijet vs. the unfolded cross sections.

Normalised Trijet Cross Section

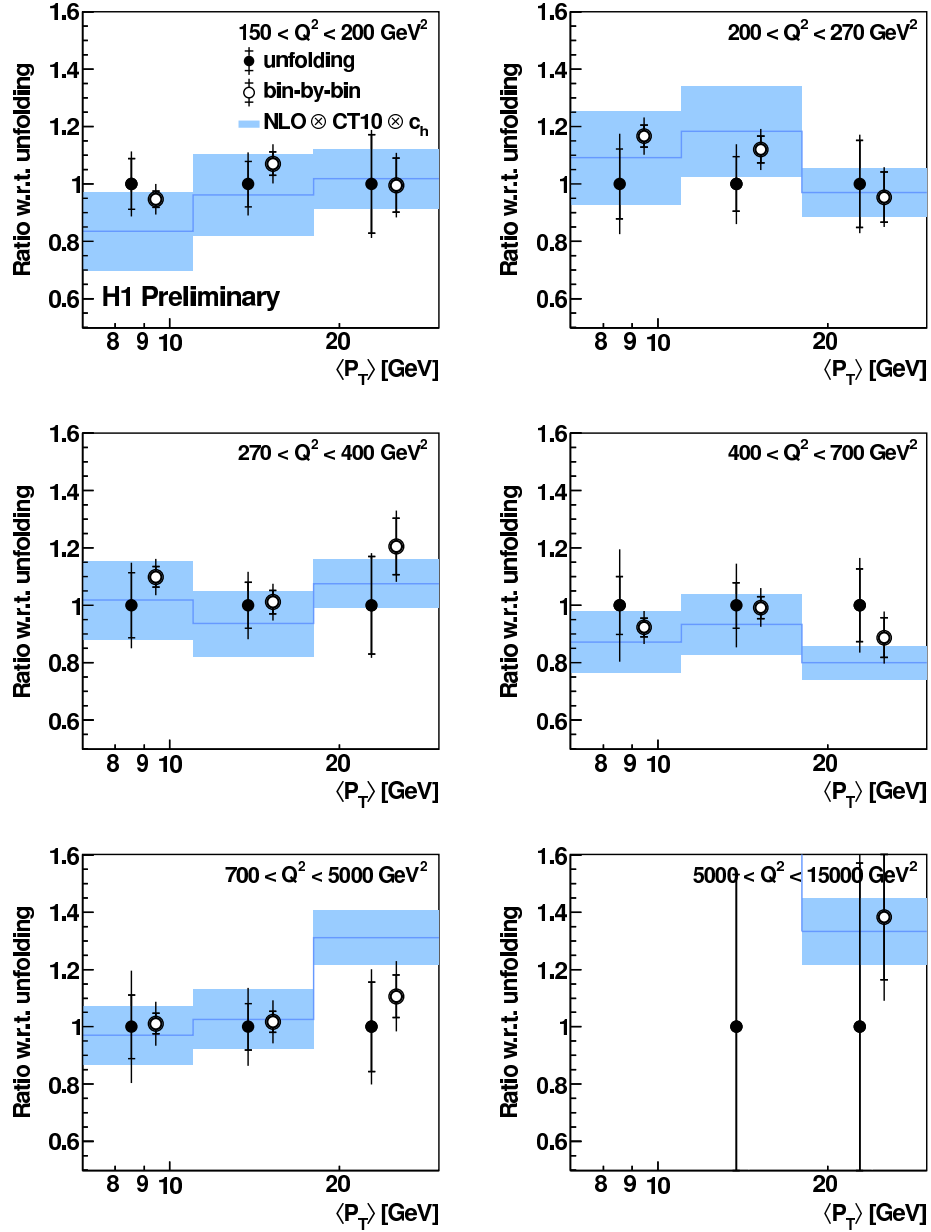


Figure 11: Ratio of the bin-by-bin corrected cross section of the normalised trijet vs. the unfolded cross sections.